Scratch Drive Actuator with Mechanical Links for Self-Assembly of Three-Dimensional MEMS

Terunobu Akiyama, Dominique Collard, and Hiroyuki Fujita, *Member, IEEE*

***Abstract*— The self-assembling of three-dimensional (3-D) MEMS from polysilicon surface micromachined part is very attractive. To avoid risky external manipulation, the practical use of integrated actuator to perform the assembling task is required. To that goal, this paper presents detailed characteristics of the electrostatic surface micromachined scratch drive actuator (SDA). First, from numerous SDA test, it results that this actuator is able to produce a threshold force of 30 μN, with a yield above 60%. With polysilicon devices consisting of SDA mechanically linked to buckling beam, a horizontal force of 63 mN have been demonstrated with $\pm$112 V pulse, and up to 100 μN can be obtain with higher voltage. With buckling beams, displacements up to 150 μm have been obtained in the vertical direction. The generation of vertical force of 10 μN was confirmed with a 100 μm displacement producing in 1 nJ work in the vertical direction. Finally, SDA proves to overcome the usual sticking of surface machined polysilicon by producing enough vertical force to completely release wide polysilicon plate (500 μm $\times$ 50 μm) without external manipulation. The above characteristic, both in terms of structure releasing and vertical/horizontal forces and displacements provide the SDA with the capability of self-assembling complex 3-D polysilicon part, opening new integration capabilities and new application field of MEMS. [214]**

***Index Terms*— Electrostatic devices, fabrication, microactuators, microelectromechanical devices, position control.**

I. Introduction

THE BATCH fabrication of three-dimensional (3-D) structures will allow the production of new kinds of sensors/actuators that will enlarge the application field of MEMS. The handling of microparts poses a major difficulty to assemble these devices automatically. In 3-D MEMS consisting of surface micromachined parts, the construction parts are usually connected to each other by mechanical hinges [1] or elastic hinges having lower stiffness than that of the constituting parts [2]. Since the hinged structure does not require complicated parts handling compared with assembling of the structure from fully separated parts, the basic assembling operation consists to lift upward the parts from the substrate to out-of-plane position. Usually, this operation is done manually by using microprobes. However, misoperation results in permanent damages of the structure, and probe manipulation is far from batch processes.

One approach to solve the problem is to develop microteleoperating robots [3]–[6]. It will remain a sequential assembly process even when such robots are fully automated. The other approach, which we have adopted in this study, is to utilize microactuators integrated with microstructures for assembly. Movement of the actuator fabricated on the same substrate has to be investigated to perform this task without giving any damages. This approach is quite attractive for self-assembling polysilicon 3-D MEMS such as microrobots [2], [7], microgrippers [8], and micro-optical systems [9], [10]. Smela *et al.* [6] demonstrated self-assembling of 3-D microstructures with active joint made of a conductive polymer. It worked, however, only in liquid, and was not fully compatible with polysilicon structures. Many polysilicon actuators, such as micromotors [11], [12], comb drive actuators [13], [14], and scratch drive actuator (SDA) [15], [16], have been studied and can be integrated on the wafers at the same time. The required characteristics for the actuators to lift up microparts are an output force in the few μN range and a displacement in the order of a few tens of μm [7]. Yeh *et al.* [7] reported that a typical force of 2 μN in the substrate plane was needed to move a hinged polysilicon part having push rods from substrate to out-of-plane against its adhesive force.

In our previous work, it has been demonstrated that SDA is capable of producing over 100 μN [16] and of moving for over 500 μm distance [15]. In addition, SDA motion can be controlled by changing the number of applied electrical pulses and its velocity can be also be tuned by changing the pulse frequency [15]. The performance of SDA is then suitable for microparts handling, and one can expect a new type of polysilicon 3-D MEMS which self-assembles with the movement of integrated SDA without external manipulation.

To illustrate our concept, Fig. 1 depicts a possible 3-D self-assembled polysilicon structure; this is a simple stage supported in out-of-plane with a permanently deformed beam. In the self-assembling process, a reshaping technology [17], as well as a movement of SDA, is used to make a permanently deformed beam. The structure is made from a polysilicon layer by the surface micromachining technology and is initially in a plane [Fig. 1(a)]. First, SDA is driven and an elastic beam is buckled. A stage is lifted into out-of-plane from a substrate with the bucking beam [Fig. 1(b)]. Then, to provide plastic deformation of the beam, a current resulting in the joule heat

Manuscript received May 29, 1996; revised September 2, 1996. Subject Editor, H. Miura. T. Aiyama was supported by the Japan Society for the Promotion Science.

T. Akiyama was with the Institute of Industrial Science, The University of Tokyo, Tokyo 106, Japan. He is now with the Institute of Microtechnology, University of Neuchâtel, Neuchâtel CH-2007, Switzerland.

D. Collard is on leave from IEMN Lille, France. He is currently with the Laboratory for Integrated Micro-Mechatronic Systems, LIMMS/CNRS-IIS, Institute of Industrial Science, The University of Tokyo, Tokyo 106, Japan.

H. Fujita is with the Institute of Industrial Science, The University of Tokyo, Tokyo 106, Japan.

Publisher Item Identifier S 1057-7157(97)01553-9.

1057–7157/97$10.00 © 1997 IEEE

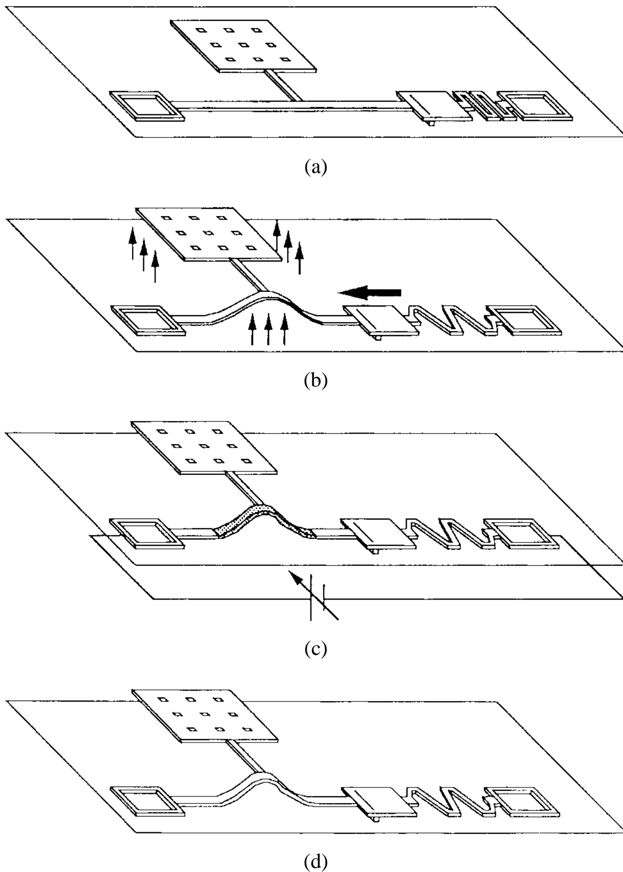

Fig. 1. Illustration of 3-D self-assembled polysilicon structure.

is applied while keeping SDA to push the beam [Fig. 1(c)]. As a result of the annealing effect, the plastic deformation of polysilicon occurs [17]. After releasing the current, the permanent 3-D microstructure is obtained [Fig. 1(d)]. In this self-assembling process, no external manipulation is required and all of this is carried out within a microworld.

To verify our concept, however, several issues about SDA characteristics have to be carefully investigated and validated, and controllable out-of-plane motion have to be demonstrated. These investigations are reported in this paper. One of the main issues is related to the appropriate dimensions of SDA. The relationship between SDA dimension and its behavior has not been theoretically clarified, yet. We provide experimental results and statistical study on the relationship between optimal SDA dimensions and output force. Then, dedicated polysilicon devices having SDA and elastic beams were realized to demonstrate that SDA can be utilized for self-assembly of 3-D MEMS. In this device, a polysilicon beam was buckled to out-of-plane position with the output force generated by a SDA. Finally, as a practical task, a small piece of quartz put on the beam was lifted up by the vertical force produced by the polysilicon device.

II. Scratch Drive Actuator

A scanning electron microscope (SEM) photograph of a typical polysilicon SDA is shown in Fig. 2. The device is on an insulator film passivated on a substrate surface. The essential part that generates a movement of the actuator is a plate having a bushing along one side. The bushing is a prominence created in the inner surface of the plate. As shown in Fig. 2, the plate is supported over the substrate by two narrow beams and two anchors. A potential is applied from outside to the plate through the anchors and the beams.

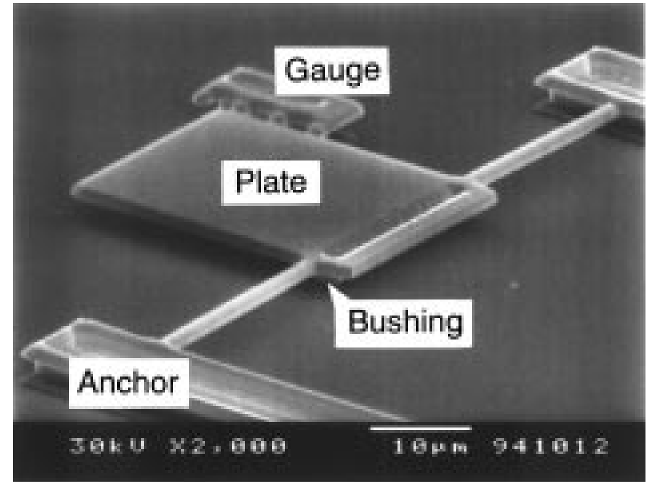

Fig. 2. SEM picture of a SDA supported by elastic beams. With the gauge, forward motion can be checked under optical microscope.

Since the plate and the substrate has a capacitor-like structure, an electrostatic force can be easily generated on the plate. A periodical electrostatic force applied to the plate results in a movement of SDA in a substrate plane as the plate having the bushing repeats a step motion, shown in Fig. 3. Fig. 3(a) gives a schematic view of the SDA and Fig. 3(b)–(e) illustrates the model of this step motion when a square pulse is applied between the plate and the substrate. Fig. 3(b) shows a cross-sectional view of the SDA when no electrostatic force is applied. At the rise of an applied pulse, the plate is pulled down to the substrate. Since there is the bushing at the front side of the plate, the whole area of the plate does not attach on the insulator and the plate is warped, as shown in Fig. 3(c). An elastic strain energy is temporarily stored in the plate. At the fall of the pulse, the elastic strain energy is released and the plate begins to restore the original shape. The attaching area of the plate becomes smaller and the plate deformation is more relaxed, as shown in Fig 3(d). During this relaxation, the rear part of the plate shifts forward as the bushing remains in contact with the insulator. At the following rise of the pulse, the plate begins to be pulled down to the substrate again. Since the rear part is the closest to the insulator, this part is quickly stuck on the insulator surface. The top of the bushing is pushed forward due to the deformation of the plate and the bushing slides on the insulator, as shown in Fig. 3(e).

While repeating this step motion, the SDA can move stepwise on the insulator, and continuously moves in a substrate plane. The resulted forward displacement of SDA is supported by the beam deformation. The SDA motion can be controlled by tuning the number of applied pulses. Its velocity is proportional to the pulse frequency and, therefore, controllable too [15]. One step (dx) of SDA is defined the distance that the SDA can be moved with an applied pulse. In

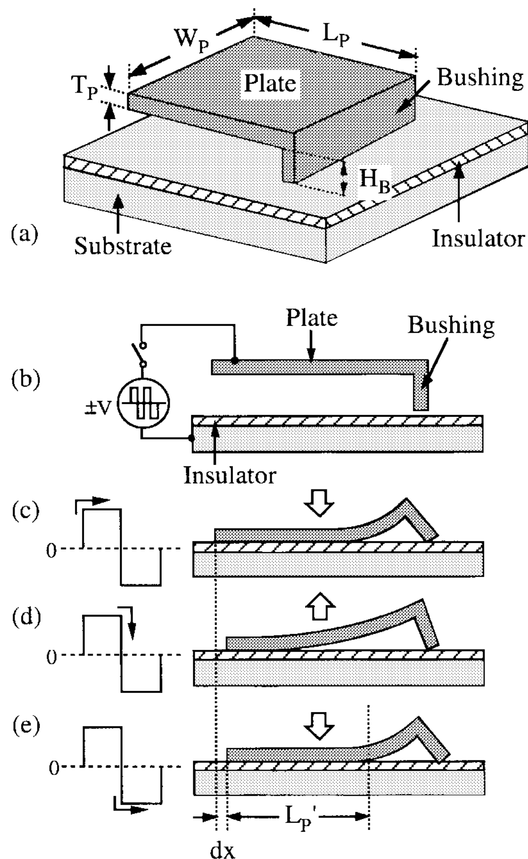

Fig. 3. (a) Schematic view of the SDA with dimension definition. (b)–(e) Model for the step motion of the SDA showing the evolution of the plate deformation according to the applied pulse, shown on the left side.

our previous work [15], it was experimentally confirmed that dx depended not only on a peak voltage of the pulse but also on both plate length and bushing height, the measured step values were in the 0.1-μm range.

III. Device Design and Fabrication

A. Design

We designed a large number of individual test SDA that were similar to the one shown in Fig. 2, to analyze the step motion and to investigate the relationship between the SDA dimension and the output force. More complex polysilicon devices for the self-assembly experiment including out-of-plane motion and for more quantitative output force analysis were also fabricated. A top view and a cross section of the polysilicon device are shown in Fig. 4. The device consists of a SDA attached to mechanical links (a link frame and a buckling beam) and a buried shield. The right end of the buckling beam is directly fixed on the shield and the left end is connected to the link frame. For this connection, two narrow and short torsion bars are provided to accommodate the difference of angles between the link frame and the beam during buckling. The driving voltage applied to the pad reaches the SDA through the plate and the mechanical parts. The shield prevents the electrostatic force to be applied on the buckling beams and to the mechanical links. In operation, the SDA moved forward and pulls the link frame having two long bushings. The output force of SDA is transmitted to the rear part of the beam that can buckle.

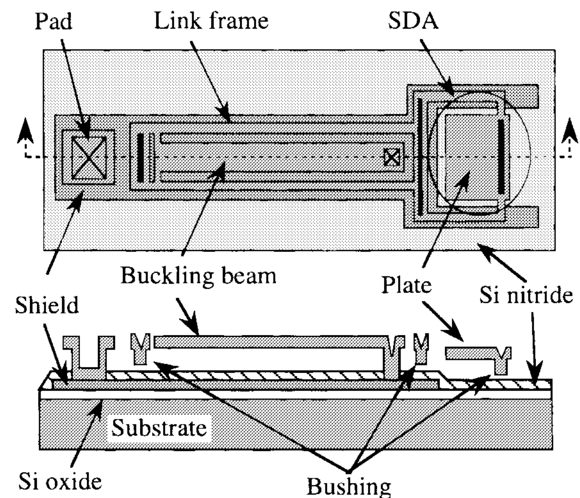

Fig. 4. Top view and cross section view of the polysilicon structure composed of a SDA with mechanical links.

B. Wafer Processing

A cross-sectional view of the SDA with mechanical links at various stages of the fabrication sequence is shown in Fig. 5. A 20-Ω cm, n-type (100) silicon wafer was prepared for the device fabrication with an initial cleaning in buffered hydrofluoric acid (BHF). After a water rinse and N_2 drying, the wafer was thermally oxidized at 1100 °C in dry O_2. A 0.35-μm-thick silicon oxide layer was grown on the wafer. A 0.5-μm-thick polysilicon layer was then deposited at 600 °C by low-pressure chemical vapor deposition (LPCVD). To reduce the polysilicon resistivity, phosphorus was implanted with a 5×10^{15} cm^{-2} dose at 50-keV acceleration voltage. After the first lithography, the polysilicon layer was patterned in a SF_6 plasma to form the shield. A 0.3-μm-thick silicon-rich silicon nitride layer was then deposited over the entire wafer surface at 800 °C by LPCVD [Fig. 5(a)]. This layer protects the silicon oxide layer from being etched by the hydrofluoric acid (HF) in the final sacrificial etching step.

Next, a 2.0-μm-thick silicon oxide layer was deposited as a sacrificial material at 600 °C by LPCVD. After the second lithography, bushing molds were patterned by reactive ion etching (RIE) with CHF_3+O_2 plasma. The depth of the bushing mold determines the SDA bushing height. With time controlled etching a 1.5-μm depth of the bushing mold was obtained. Therefore, the clearance of 0.5 μm appears between the bushing and the nitride layer in a released device. The third lithography for contact was then performed. In the contact area, both LPCVD silicon oxide and silicon nitride was removed by RIE with CHF_3+O_2 plasma [(Fig. 5(b)] so that subsequent deposited polysilicon can locally contact the buried shield layer.

A 1.0-μm-thick polysilicon layer which would be patterned as a main component was deposited on the wafer surface at 600 °C by LPCVD. The thickness of both SDA and buckling

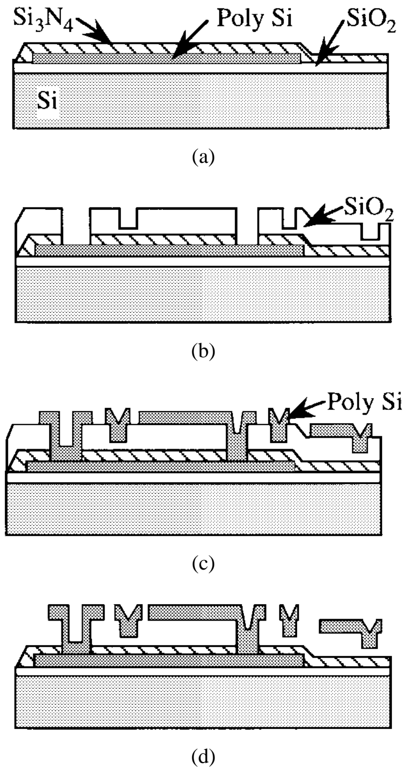

Fig. 5. Fabrication steps of the polysilicon device. (a) After shield patterning and isolation. (b) After bushing patterning and contact hole formation. (c) After structural polysilicon patterning. (d) Final device after releasing.

beams was determined by this polysilicon thickness. This structural polysilicon layer was doped by phosphorus implant (5×10^{15} cm^{-2}, 150 keV) and was delineated by RIE with SF_6+ $SiCl_4$ plasma in the fourth lithographic step [Fig. 5(c)].

To release the residual stress of the polysilicon, the wafer was heated in N_2 at 1100 °C for 60 min after a thin LPCVD silicon oxide deposition. This silicon oxide layer was used to prevent the polysilicon surface to be roughed by heated nitrogen. At the same time, the activation and diffusion of phosphorus in the polysilicon were carried out. Finally, the wafer was dipped into 50% HF to fully dissolve the sacrificial silicon oxide. The wafer was rinsed in DI water and isopropyl alcohol (IPA), and dried carefully in N_2 blow, and the process was completed [Fig. 5(d)].

C. Fabricated Devices

The test SDA with different dimensions and the polysilicon devices for the self-assembly experiment were fabricated at the same time through the fabrication process described above. Fig. 6 shows a typical photograph of the test SDA that was taken during the yield investigation described in the next chapter. SDA with various plate lengths L_P are arrayed and form a column, as shown in Fig. 6. SDA with different plate widths W_P are implemented in adjacent columns. L_P varies in the 30 μm $\sim$ 100 μm range while W_P values were set to 50 μm, 75 μm, and 100 μm. The plate thickness T_P (that is a process parameter) is set at $T_P = 1$ μm. The bushing height H_B that is also process dependent was chosen as $H_B = 1.5$ μm.

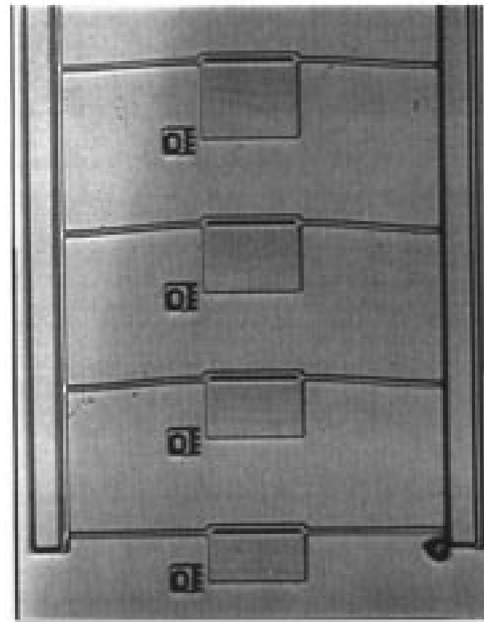

Fig. 6. View from an optical microscope of a typical test column of SDA. From the bottom, second, third, and fourth SDA are considered operational.

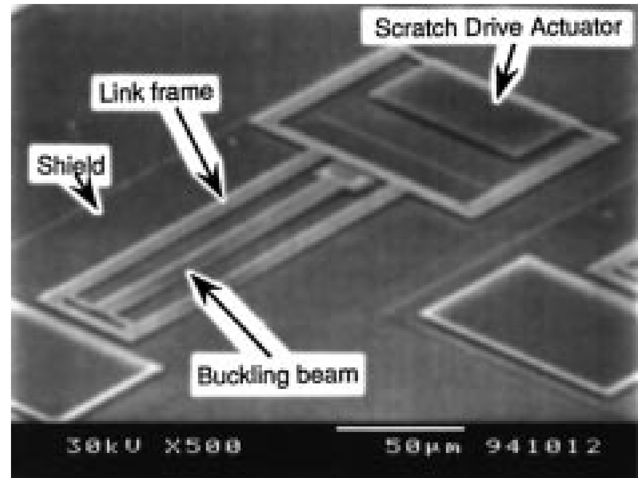

Fig. 7. SEM photograph of the polysilicon device including a SDA actuator and a mechanically linked buckling beam.

Fig. 7 shows a SEM photograph of a typical polysilicon device with mechanical links. Three kinds of SDA with different dimensions were designed; $L_P = 60$ μm, 80 μm, 100 μm for $W_P = 75$ μm. Additionally, for each SDA type, five beams with different dimensions were designed. The dimension of the beams varies from 200 μm to 500 μm in length, and from 10 μm to 30 μm in width. The beam thickness is set constant to 1.0 μm.

IV. Experimental Results

A. Yield Versus Dimension of SDA

We tried to find the SDA having the most appropriate dimension for self-assembling 3-D MEMS, as shown in Fig. 1. All the individual test SDA, as shown in Fig. 2, have the same

suspension beams. Considering that the beam deflection is only a function of the output force of SDA, we could estimate directly the amount of output force by measuring the deflection. However, the two suspension beams that support the SDA do not always bend symmetrically, resulting in a small rotation of SDA and making individual measurement inaccurate. So, a large number of SDA have to be tested to improve the accuracy of the measurement. Moreover, considering the self-assembling structure like in Fig. 1, the largest force of SDA is required only for providing a beam being buckled. Therefore, we defined a threshold force and examined whether a SDA was capable of generating this force or not. In fact, a displacement of SDA was taken into account. By evaluating the yield of the devices which could exceed the threshold and by comparing the yield for different sizes, we obtained the optimal dimension range of SDA.

We set the threshold force of 30 μN, which corresponds to a deflection of the beams of 4 μm. This is because the force range, which is required to buckle the five beams in the devices for the buckling experiment is 10 μN $\sim$ 63 μN. The threshold force is within the range and equal to the force to buckle one of five beams.

The sinusoidal signal at 50 Hz with maximum peak voltage of 150 V was applied to test devices. Fig. 6 shows a typical test result, when the equilibrium between the output force and the beam bending was reached. From bottom, the second, third, and fourth SDA are considered generating a larger force than a threshold force.

Fig. 8 shows the relationship between the yield and the dimensions of SDA. In Fig. 8, the yield is given in terms of the SDA length L_P for the three different widths W_P. For all SDA lengths, the number of tested devices was 35, 32, and 36, for W_p equals to 50 μm, 75 μm, and 100 μm, respectively. From Fig. 8, it is clearly seen that the SDA having a width of 50 μm has a lower yield than the others. On the other hand, no essential yield difference is found between the SDA having widths of 75 μm and 100 μm. We believe that the threshold force was not high enough to distinguish the difference between these two widths; it is likely that SDA having wider plate can generate larger output force. If we want better yield than 60%, SDA lengths L_P, ranging from 35 μm to 60 μm, are suitable.

The step motion can be also analyzed by measuring the SDA plate deflection during the step motion. Fig. 9 gives the temporal evolution of the attached plate length L'_P resulting from an applied triangular voltage on three SDA having lengths equals to 60, 70, and 80 μm. L'_P was obtained to observe interference color of the SDA plate by an optical microscope and a video system. In this plot, for each SDA the time origin was set at the moment when the SDA plate begins to relax its deformation after a given fall of the bias, as shown in the legend sketch. For the shorter SDA, $L_P = 60$ μm, the plate relaxation is quite complete, and the force resulting from the step motion exceeds the threshold force value; this is consistent with the high yield as shown in Fig. 8. In the other hand, for the longer device, the relaxation is not completely achieved, and a large attachment remains even after a complete fall of the pulse, respectively 35 and 50 μm for the 70- and

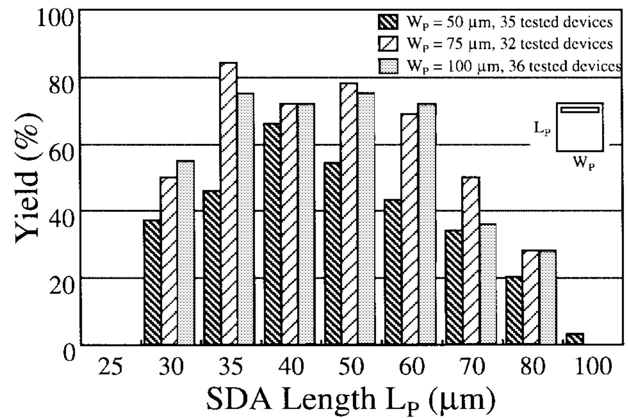

Fig. 8. Yield plot for three different SDA widths. The yield is given by the ratio between the number of SDA producing an output force greater than 30 μN and the number of tested SDA.

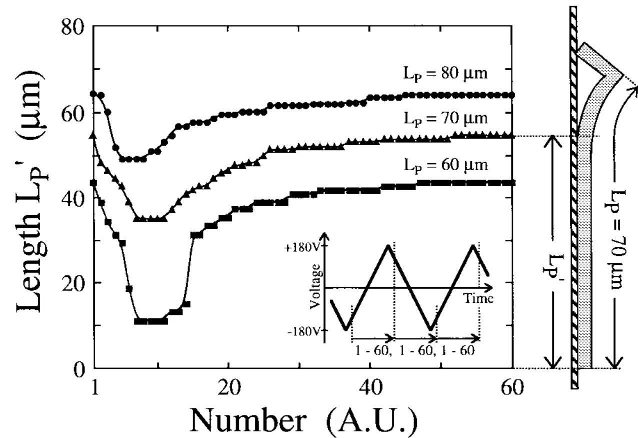

Fig. 9. Temporal evolution of the SDA attachment length with a triangular excitation. The evolution of three SDA with different length are plotted. For each SDA, the time origin is at the beginning of the plate relaxation after a given fall of the maximum voltage, that is indicated by the dashed line in the sketch. These measurements were made from interferometric fringe motion survey from video recording with an optical microscope.

80-μm-long devices. This incomplete step motion, due to a lower stored mechanical energy, is directly responsible of the lower yield in Fig. 8.

B. Beam Buckling

Some of the devices for the self-assembly experiment (like those shown in Fig. 7) suffer from the sticking problem of the beams on the underneath insulator before they were tested. In Fig. 7, not only the buckling beam but also the mechanical frame stuck on the under layer. This problem is likely to happen in all surface micromachined devices. Therefore, whether the SDA can release (or not) the beams from the insulator surface is a crucial issue to overcome for the self-assembling structure.

Though we designed three kinds of SDA with different dimensions, only one kind ($L_P = 60$ μm, $W_P = 75$ μm) could release all the five beams with different dimension from the insulator surface with a pulse having a peak voltage of 200 V (limit voltage of our equipment). Other two kinds of SDA could not release them at all, although they could provide a

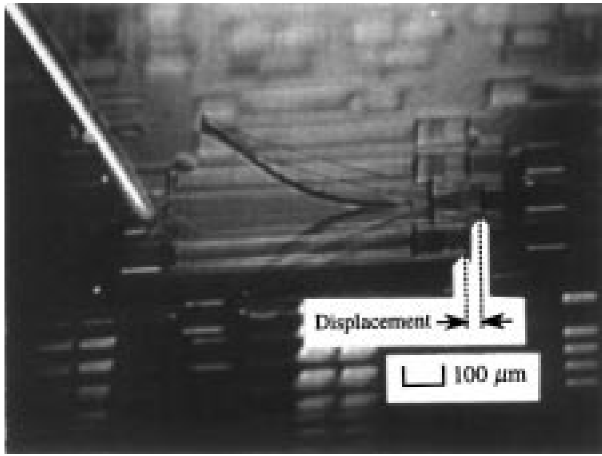

(a)

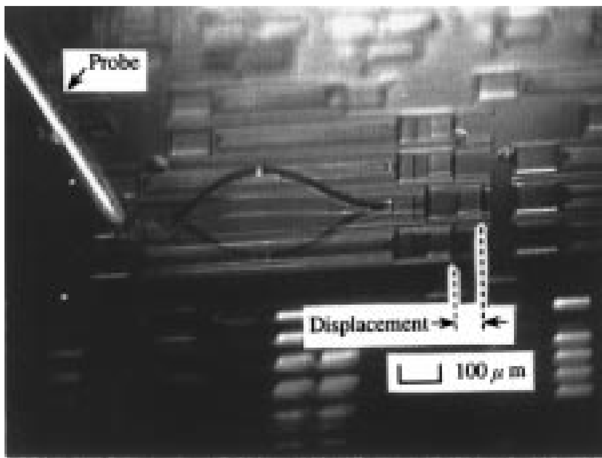

(b)

Fig. 10. Photographs of the beam buckling experiment obtained with the polysilicon devices. The SDA is on the right part of the device. (a) Releasing of the beam with the motion of the SDA. (b) Buckling beam situation for the quantitative force evaluation.

beam buckling if the beam is not suffered from sticking. This result is in agreement with the result of yield measurement in Fig. 8. With a square pulse having a maximum peak voltage of 140 V at 50 Hz, the most powerful SDA could release all the five beams. As soon as the SDA started to move forward, the sticking beams were released and bent, as shown in Fig. 10(a). The largest beam (500 μm $\times$ 50 μm) in this experiment was also released without any problem. Once the applied voltage was removed, the beams and the SDA sprang back to their original position. The sticking problem was no longer observed. Applying the bias again, we could bend the beams as shown in Fig. 10(b). With 50-Hz pulse frequency, a typical velocity of the SDA motion having a long and narrow beam (500 μm $\times$ 10 μm) was 8 μm/s, while the beam is bending as shown in Fig. 10(b). The average step for one pulse is therefore estimated as $dx = 80$ nm. For a pulse frequency of 250 Hz, the beam bending experiments showed both shapes of Fig. 10.

During buckling experiment, as shown in Fig. 10(b), the highest point of the beam bending was measured as a function of the SDA displacement. Fig. 11 gives the results for three

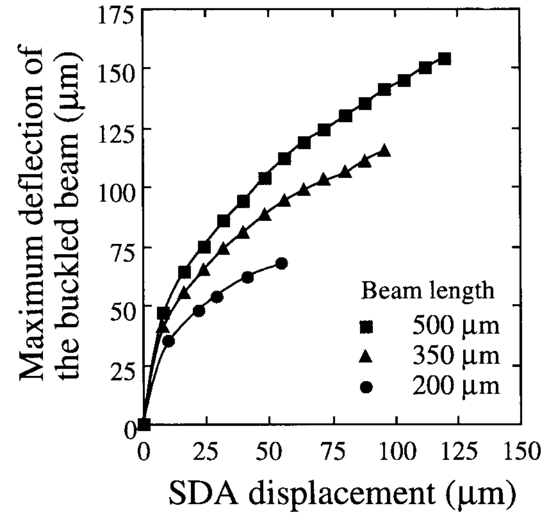

Fig. 11. Maximum deflection of the buckled beam versus the horizontal SDA displacement.

different beam lengths. It can be seen that we obtain a larger out-of-plane displacement, perpendicular to the substrate, than the SDA displacement in the substrate plane. This experimental observation is very promising for 3-D structure self-assembly. It was also found, for this devices, that the maximum deflection of beams always reach up to 30% of the beam length. When we wanted to obtain larger deflection, the fixed end attachment of the buckling beam was always broken due to excessive deformation.

C. Force

When the output force is not larger than the critical force P_{crit}, which is required to provide the buckling of the beam, the SDA cannot move forward and the structure cannot deformed. At the moment when the beam begins to buckle, the output force of the SDA is considered to be equal to P_{crit}. Thus, by checking the buckling capability, a quantitative relationship between the peak voltage of the pulse and the output force of SDA can be established. Once the beam is buckled, not so much force as P_{crit} is required to enhance the deformation of the beam. The reason why we used this structure, but not one like shown in Fig. 6, to obtain the relationship is that the device has the most practical configuration for implementation of a self-assembling microstructure. Since wear of both polysilicon and nitride is likely to occur with the scratching motion, we also considered it as important that SDA does not step in forward and repeats the scratching motion at the position until the output force reaches to P_{crit}. P_{crit} is given by the Euler's equation as follows [18]:

$$P_{\text{crit}} = \frac{C\pi^2 EI}{l^2} \tag{1}$$

where C is a constant which depends on a shape of the buckled beam, E is the Young's modules of material, I is a moment of inertia of the cross-sectional area, and l is the beam length. $C = 0.25$ when the beam is buckled as Fig. 10(a) and $C = 2$ for the case of Fig. 10(b). In the calculation $E = 150$ GPa, which is obtained for our polysilicon film

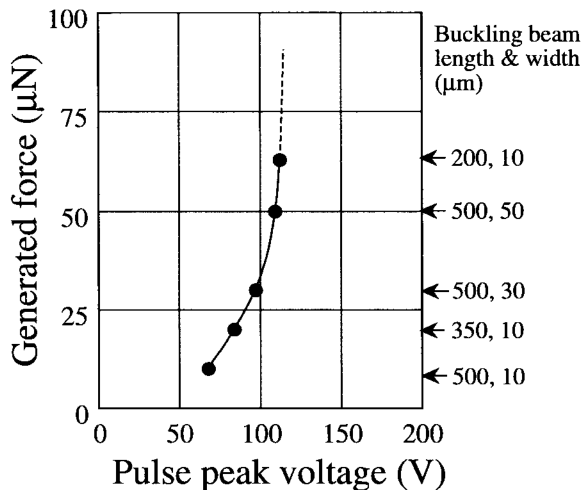

Fig. 12. Evolution of the generated force produce by the SDA and the peak value of the applied voltage. The size of the corresponding buckled beam is also mentioned in the right side.

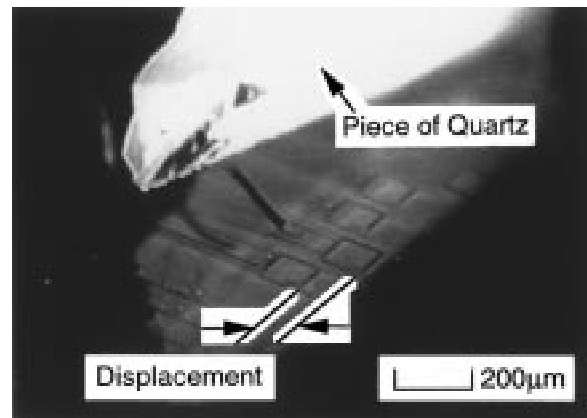

Fig. 13. A photograph of the polysilicon device lifting up a triangular piece of quartz.

in an experiment using simple test structures, is assumed for the Young's modules.

A programmable pulse generator was used to make a square pulse whose peak voltage is gradually increased from 0–200 V. The frequency was fixed at 50 Hz and a voltage increasing rate of 10 V/s was chosen. The results are summarized in Fig. 12. Five devices were used. The size of the beams for each device is shown at the right side of the figure. The output force of SDA is radically increased with the increase of the pulse peak voltage. For the voltage increasing from 68–112 V (about two times), the output force increases from 10 μN to 63 μN (about six times). Since the SDA is capable of being operated at 200 V, the maximum output force of SDA may reach the order of 100 μN. This maximum value is in agreement with estimation deduced from the yield experiment of Fig. 8.

In the absence of the quantitative SDA model, we can not exactly explain the reason of the radical increasing of output force. However, we consider it as follows. There is the flat part in SDA plate that is always attaching to the insulator during the step motion (see Fig. 9). For SDA stepping in forward, a part of the elastic energy stored in the deformed part of the plate is used to overcome the friction of the flat part, and the rest is used to pull the mechanical links during the relaxation of SDA plate. This can be deduced from the experiment results in Figs. 8 and 9, i.e., for the longer SDA plate the friction is also larger, and the SDA force is not so powerful. Therefore, if we consider the friction force as a threshold it can be supposed that the output force of SDA is nearly zero below the threshold and increases radically with the pulse peak voltage over the threshold. We would like to investigate the mechanism of generating force of SDA in our future work.

D. External Work Produced by the Buckling Beam

We put a piece of quartz on the wafer and tried to lift it from the substrate to investigate the out-of-plane performance of the SDA with mechanical links. Fig. 13 shows the photograph of a lifted piece. The top view of the piece was an acute-angled triangle with side lengths of 4.2 mm, 4.2 mm, and 1.7 mm. The thickness of the piece was 0.3 mm, and its weight was about 2.2 mg. The acute angle corner was lifted up to 75 μm while the other corners stayed on the substrate. The applied square pulse was 140 V at 50 Hz. The buckling beam size in this experiment was 500 μm $\times$ 30 μm.

Finally, to evaluate the vertical force that this device can generate on an external object, we tried to put a small weight directly on the highest point of the buckling beam. A very short needle with a simple support was prepared for the purpose. Initially, the tip of the needle was set at 20 μm above the substrate. The needle was successfully pushed upward, and a vertical displacement of approximately 100 μm was obtained. The corresponding weight is about 1 mg and, so, a typical generated upward force of 10 μN was confirmed. The total vertical work that this device could produce was about 1 nJ, that make it very competitive for 3-D structure self-assembly.

V. Conclusion

It was proposed that an integrated actuator was utilized for 3-D polysilicon device self-assembling. The performances of the SDA for the purpose have been quantitatively investigated in this paper. From test of numerous SDA, it was found that SDA having plate lengths in the 35–60 μm range were able to produce a threshold force of 30 μN, with a yield above 60%. The output force increased with the SDA width. With polysilicon devices consisting of SDA mechanically linked to buckling beam, a horizontal force of 63 μN was demonstrated with $\pm$112 V pulse and up to 100 μN could be obtained with higher voltage. During these experiments, out-of-plane displacement of the highest point of the beam was found to be greater than the SDA horizontal displacement, a maximum value of 150 μm was obtained in the vertical direction. These devices were even able to lift a corner of a triangular piece having a weight of 2.2 mg up to 75 μm. And finally, with a very short needle placed on the beam apex, a vertical force of 10 μN was confirmed with a 100 μm displacement producing in 1 nJ work in the vertical direction. Moreover, the SDA allows to overcome the usual sticking of surface machined polysilicon parts by producing enough vertical force and to

completely release wide polysilicon plate (500 μm × 50 μm) without external manipulation.

The above characteristic, both in terms of structure releasing and vertical/horizontal forces and displacements provide the SDA with the capability of self-assembling complex 3-D polysilicon part. The polysilicon device, consisting of a SDA, mechanical links, and buckling beams, is already a basic self-assembling 3-D device in a sense that the 3-D dimension is easily controlled by the horizontal motion of the SDA.

All the demonstrated capabilities of the integrated SDA now allows the investigation of the automatic self-building of complex 3-D MEMS from surface micromachined parts, opening new integration capabilities and new application field of MEMS.

REFERENCES

[1] K. S. J. Pister, "Hinged polysilicon structures with integrated CMOS TFT's," in *Tech. Dig. IEEE Solid-State Sensor Actuator Workshop*, Hilton Head Island, SC, June 1992, pp. 136–139.

[2] K. Suzuki, I. Shimoyama, and H. Miura, "Insect-model based microrobot with elastic hinges," *J. Microelectromech. Syst.*, vol. 3, no. 1, pp. 4–9, Mar. 1994.

[3] H. Miyazaki and T. Sato, "Fabrication of 3-D quantum optical devices by pick-and-place forming," in *Proc. IEEE Microelectromech. Syst.*, San Diego, CA, Feb. 1996, pp. 318–324.

[4] Y. Hatamura, M. Nakao, T. Sato, K. Koyano, K. Ichiki, S. Sangu, M. Hatakeyama, T. Kobata, and K. Nagai, "Construction of 3-D microstructure by multiface fab, cofocus rotational robot, and various mechanical tools," in *Proc. IEEE Microelectromech. Syst.*, Oiso, Japan, Jan. 1994, pp. 297–302.

[5] A.-L. Tiensuu, M. Bexell, J.-Å. Schweitz, L. Smith, and S. Johansson "Assembling three-dimensional microstructures using gold-silicon eutectic bonding," *Sensors Actuators*, vol. A-45, pp. 227–236, Dec. 1994.

[6] E. Smela, O. Lungans, and I. Lundstrm, "Controlled folding of micrometer-size structures," *Sci.*, vol. 268, pp. 1735–1738, June 1995.

[7] R. Yeh, E. J. J. Kruglick, and K. J. Pister, "Microelectromechanical components for articulated microrobots," in *Tech. Dig. Transducers '95*, Stockholm, Sweden, June 1995, pp. 346–349.

[8] G. Lin, K. S. Pister, and K. P. Roos, "Standard CMOS piezoresistive sensor to quantify heart contractile forces," in *Proc. IEEE Microelectromech. Syst.*, San Diego, CA, Feb. 1996, pp. 150–151.

[9] M.-H. Kiang, O. Solgaard, R. S. Muller, and K. Y. Lau, "Surface-micromachined electrostatic-comb driven scanning micromirrors for barcode scanners," in *Proc. IEEE Microelectromech. Syst.*, San Diego, CA, Feb. 1996, pp. 192–197.

[10] L. Y. Lin, S. S. Lee, M. C. Wu, and K. J. Pister, "Micromachined integrated optics for free-space interconnections," in *Proc. IEEE Microelectromech. Syst.*, Amsterdam, The Netherlands, Feb. 1995, pp. 77–82.

[11] K. Deng, M. Mehregany, and A. S. Dewa, "A simple fabrication process for polysilicon side-drive micromotors," *J. Microelectromech. Syst.*, vol. 3, no. 4, pp. 127–133, Dec. 1994.

[12] R. Legtenberg, E. Berenschot, M. Elwenspoek, and J. Fluitman, "Electrostatic microactuators with integrated gear linkages for mechanical power transmission," in *Proc. IEEE Microelectromech. Syst.*, San Diego, CA, Feb. 1996, pp. 204–209.

[13] M. J. Daneman, N. C. Tien, O. Solgaard, A. P. Pisano, K. Y. Lau, and R. S. Muller, "Linear microvibromotor for positioning optical components," in *Proc. IEEE Microelectromech. Syst.*, Amsterdam, The Netherlands, Feb. 1995, pp. 55–60.

[14] A. Selvakumar, K. Najafi, W. H. Juan, and S. Pang, "Vertical comb array microactuators," in *Proc. IEEE Microelectromechm Syst.*, Amsterdam, The Netherlands, pp. 43–48, Feb. 1995.

[15] T. Akiyama and K. Shono, "Controlled stepwise motion in polysilicon microstructures," *J. Microelectromech. Syst.*, vol. 2, no. 3, pp. 106–110, Sept. 1993.

[16] T. Akiyama and H. Fujita, "A quantitative analysis of scratch drive actuator using buckling motion," in *Proc. IEEE Microelectromech. Syst.*, Amsterdam, The Netherlands, Feb. 1995, pp. 310–315.

[17] Y. Fukuta, T. Akiyama, and H. Fujita, "The reshaping technology for three dimensional polysilicon microstructures," *Inst. Elec. Eng. J. Trans. E Sensors Micromachines*, to be published.

[18] J. M. Gere and S. P. Timoshenko, *Mechanics of Material*, 3rd ed. Boston, MA: PWS-Kent, 1990.

Terunobu Akiyama was born in Tokyo, Japan, on October 10, 1966. He received the B.S., M.S., and Ph.D. degrees in electrical and electronic engineering, in 1989, 1991, and 1994, respectively, all from Sophia University, Tokyo, Japan.

From 1994 to 1995, he was with the Institute of Industrial Science at the University of Tokyo, Japan, and from 1995 to 1996, he was with the Institute of Microtechnology at University of Neuchtel, Switzerland, both as a Post Doctoral Fellow. He is currently a Research Assistant at the Institute of Microtechnology, University of Neuchâtel, Switzerland. His research interests includes microactuators, microsystems, and microsensors.

Dr. Akiyama received the Research Fellowships of the Japan Society for the Promotion of Science for Young Scientists in 1994.

Dominique Collard was born in Cambrai, France, in 1958. He received the Eng. degree from ISEN in 1980, and the Ph.D. degree from the University of Lille, France, in 1984.

From 1985 to 1986, he was with TOSHIBA ULSI Research Center in Kawasaki, Japan, as Visiting Scientist. He entered the Centre National de la Recherche Scientique (CNRS) as a Senior Researcher in 1988, and settled a research group on silicon process and device simulation at ISEN (Institut Superior d'Electronique du Nord) and IEMN (Institut d'Electronique et du Microélectronique du Nord), Lille, France, his own research activity focused on silicon oxidation simulation and related mechanical stress effects. Since January 1995, he has been with the Laboratory of Integrated MicroMechatronic Systems Joint Laboratory (LIMMS), Tokyo, Japan, between CNRS and the Institute of Industrial Science, The University of Tokyo. He is currently Director of LIMMS and works on silicon-based electrostatic microactuator for device alignment system.

Hiroyuki Fujita (S'76–M'80) received the B.S., M.S., and Ph.D. degrees in electrical engineering from the University of Tokyo, Japan, in 1975, 1977, and 1980, respectively.

In 1980, he joined the Institute of Industrial Science at the University of Tokyo as an Associate Professor, where he investigated acoustic emission phenomena from fatigue cracking of metals and electrical discharges in solid insulators. From July 1983 to June 1985, he was with the Francis Bitter National Magnet Laboratory, Massachusetts Institute of Technology (MIT), Cambridge, MA, as a Visiting Scientist, where his research activities were acoustic emission monitoring of superconducting magnets and cryomechanics and the study of the mechanical properties of materials at cryogenic temperature. He is currently a Professor at the Institute of Industrial Science at the University of Tokyo. His current research interests include micromachining technology, microactuators, and micromechatronics.

Dr. Fujita is a member of the Japanese Society of Cryogenic Engineering and the Japanese Institute of Electrical Engineering. He is an Associate Editor of the *Journal of Microelectromechanical Systems*.